Available online at www.sciencedirect.com
ScienceDirect
Continental Shelf Research 27 (2007) 2014–2031
CONTINENTAL SHELF RESEARCH
www.elsevier.com/locate/csr

Modeling the formation of undulations of the coastline: The role of tides

M. van der Vegt[a,1], H.M. Schuttelaars[b,2], H.E. de Swart[a,*]

[a]*Institute for Marine and Atmospheric research (IMAU), Utrecht University, Princetonplein 5, 3584 CC Utrecht, The Netherlands*
[b]*Environmental Hydrogeology Group, Department of Earth Sciences, Budapestlaan 4, 3584 CS Utrecht, The Netherlands*

Received 13 February 2006; received in revised form 13 April 2007; accepted 23 April 2007
Available online 18 May 2007

Abstract

An idealized model is developed and analyzed to investigate the relevance of tidal motion for the emergence of undulations of a sandy coastline. The model describes feedbacks between tidal and steady flow on the inner shelf, sand transport in the nearshore zone and an irregular coastline. It is demonstrated that an initially straight coastline can become unstable with respect to perturbations with a rhythmic structure in the alongshore direction. The mechanism causing the growth of these perturbations is explained in terms of vorticity concepts. The relative importance of tide-related and wave-driven sediment fluxes in generating undulations of the coastline is investigated for the Dutch coast. Using parameter values that are appropriate for the Dutch coast it is found that tides can render a straight coastline unstable. The model predicts a fastest growing mode (FGM) with a wavelength that is in the order of the observed length of barrier islands. The mode grows on a time scale of 50 yr and it migrates 200 m per year. The wavelength of the FGM decreases with increasing amplitude of the tidal currents. This result is consistent with data of tides, waves and the lengths of barrier islands that are located along the Dutch and German Wadden coast.

Keywords: Coastal morphology; Barrier Island; Tidal currents; Wadden Sea

1. Introduction

A large part of the world's sandy coastlines shows alongshore rhythmic variations on a wide range of length and time scales (Ehlers, 1988; Komar, 1998). This paper focuses on rhythmic mesoscale variations of sandy coasts, i.e., with a characteristic length scale in the alongshore direction of a few kilometers to tens of kilometers. Such mesoscale variations include shoreline sand waves (Bruun, 1954; Thevenot and Kraus, 1995; Ruessink and Jeuken, 2002) and sequences of barrier islands along the Dutch, German and Danish Wadden coast (Fig. 1). Here, the typical length of the barrier islands ranges between a few kilometers (Rottumeroog) and 30 km (Texel). It has been noted that the typical length of the barrier islands is inversely related to the tidal range (Oost and de Boer, 1994).

*Corresponding author. Tel.: +31 30 2533275; fax: +31 30 2543163.
E-mail address: h.e.deswart@phys.uu.nl (H.E. de Swart).
[1]Now at Section of Hydraulic Engineering, Delft University of Technology, Stevinweg 1, 2628 CN Delft, The Netherlands.
[2]Now at Department of Applied Mathematical Analysis, Delft University of Technology, Mekelweg 4, 2628 CD Delft, The Netherlands.

0278-4343/$ - see front matter © 2007 Elsevier Ltd. All rights reserved.
doi:10.1016/j.csr.2007.04.006

Fig. 1. Map showing the barrier islands along the Dutch, German and Danish Wadden coast.

The tidal range increases when moving from the Dutch Wadden Sea towards the German Bight. A similar relation between tidal range and the length of the barrier islands is found for other barrier coasts, e.g., that of Georgia Bight at the east Atlantic coast of the USA (FitzGerald, 1996).

The general objectives of the present study are twofold. The first is to gain fundamental knowledge about the origin of the observed rhythmic mesoscale variations of the coastline. The second is to derive a quantitative relationship between the characteristic length of these undulations and physical control parameters (like tidal, wave and shelf characteristics). In the past, several models were developed to analyze the dynamics of coastlines which are influenced by waves. They are all one-line models, i.e., the complex three-dimensional dynamics is parameterized, resulting in an equation for the coastline position only. A widely used one-line model is the one described by Komar (1998) (originally from Pelnard-Considère, 1956). It is based on the idea that obliquely incident waves break in the surf zone and drive a current which transports sediment. Alongshore variations in this sediment transport result in changes of the position of the coastline. Upon assuming that the width of the surf zone is constant and by only considering small deviations of the position of the coastline with respect to its alongshore mean, a diffusion equation for the position of the coastline is obtained. The diffusion coefficient is a function of the wave characteristics at the breaker line and the angle between the direction of the wave rays at breaking and the normal of the local (unperturbed) coastline. A positive (negative) diffusion coefficient implies that a small initial perturbation of the coastline will decay (grow). A negative diffusion coefficient is obtained when the angle between wave rays at breaking and the normal of the local coastline is more than 45°.

The traditional one-line model was extended by Ashton et al. (2001) and Falqués (2003). They

assumed that a change in the position of the coastline results in a change of the entire bathymetric profile. Hence, even far offshore wave properties will depend on the actual position of the coastline. The diffusion coefficient is now calculated as a function of the wave characteristics far offshore. The results of Falqués (2003) show that the diffusion coefficient in the model of Komar (1998) is always positive because the waves refract such that the wave rays at breaking will have an angle of less than 45° with respect to the normal of the local coastline. Nevertheless, in these models a straight coastline can be unstable because they account for alongshore variations in the wave height at the breaker line. It turns out that perturbations of the coastline can grow if wave rays in deep water have an angle of more than 42° with respect to the normal of the local coastline (high-angle wave instability).

The models of Ashton et al. (2001) and Falqués (2003) yield interesting new insights, but they have the drawback that they assume that even far from the coast large variations of bathymetric contours exist that are related to undulations of the coastline. Falqués and Calvete (2005) modified this by assuming that a perturbation in the position of the coastline results in a perturbation of the bottom profile with finite cross-shore extent. This model still includes the high-angle wave instability mechanism. However, for the Dutch coast waves are hardly able to trigger undulations of the coastline (Ashton et al., 2003; Falqués and Calvete, 2005). Only by using a specific shape function of the topographic perturbations induced by the undulations of the coastline (case C in Falqués, 2006) growing undulations of the Dutch coastline are found.

The considerations above motivate the development and analysis of a process-based one-line model to investigate whether tides can cause the initial formation of undulations of the coastline. If so, the length scale of the undulations could set the spacing between different inlets along a barrier coast. This idea elaborates on knowledge (see Bruun and Gerritsen, 1960; FitzGerald, 1996) that inlets form during severe storms when a barrier and backbarrier area are completely inundated and channels are cut. It seems plausible that along an undulating barrier the channels will form at locations where the barrier is retreated.

This idea will be explored in the present study and compared with another explanation for inlet spacing (FitzGerald, 1996). The latter is based on the assumption that, for a given lagoon system with a fixed distance between barrier and the coast, each inlet has the same tidal prism (which is proportional to tidal range and area of the backbarrier basin). Hence, a larger tidal range implies smaller distance between inlets. The assumptions made in that model are justifiable for the east coast of the US, but they are not valid for the Dutch and German Wadden coast.

In Section 2, a model is formulated in which coastline undulations develop as free instabilities of an alongshore uniform coastline. The new aspect of this model is that it explicitly accounts for the influence of tidal currents on the stability of the coastline. In Section 3, the basic state is described and the linear stability analysis is discussed. The model calculates the growth rate and phase speed of the coastline perturbation for different alongshore wavelengths of the perturbation. The results of this linear stability analysis are presented in Section 4. The wave–induced sand fluxes are adopted from Falqués (2006). In Section 5, a physical interpretation of the results (focusing on tidal effects) is given. Section 6 discusses whether the results of the combined wave–tide model provide an explanation for the observed spacing between successive inlets along the Dutch and German Wadden coast. Finally, in Section 7 the conclusions are given.

2. Model formulation

In this study, a Cartesian coordinate system is adopted with the x-axis pointing in the cross-shore direction, the y-axis coinciding with the alongshore mean position of the coastline and the z-axis pointing in the upward vertical direction. The domain of the model consists of three regions, viz. the surf zone, the nearshore zone and the inner shelf (Fig. 2). The surf zone is the area where the waves break and is located between the coastline $x = x_c$ and the breaker line $x = x_b$. The nearshore zone is the area where bottom changes occur due to changes in the position of the coastline and is located between the coastline $x = x_c$ and the transition line $x = x_t$, with $x_t > x_b$. Here, the transition from the nearshore zone to the inner shelf occurs. The inner shelf is the region that is located between the nearshore region and the outer shelf. The time scale of bathymetric changes in this area is large compared to that of the bottom changes in the nearshore zone.

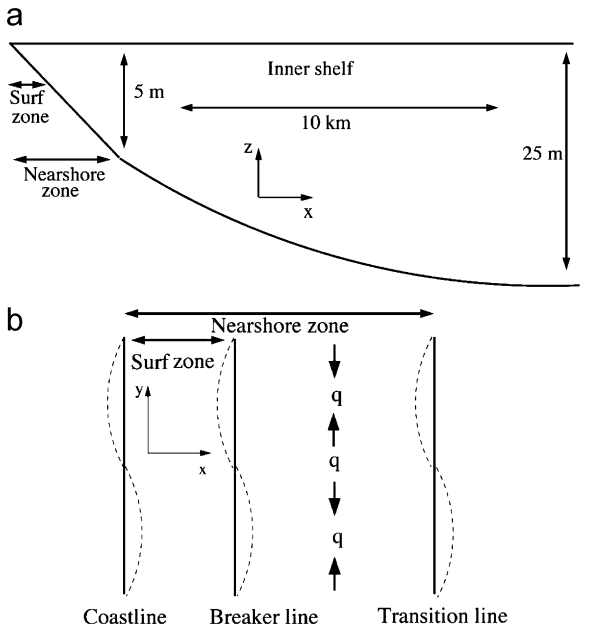

Fig. 2. (a) Side view of the geometry of the model; (b) top view of the model. The positions of the perturbed coastline, breaker line and transition line are indicated by dashed curves. It is assumed that the width of the nearshore zone is constant. The volumetric sediment flux in the alongshore direction is denoted by symbol q and occurs over the entire nearshore zone.

2.1. Hydrodynamics

The tidal hydrodynamics at the inner shelf are governed by the depth-averaged, shallow water equations. The water motion is forced by the semi-diurnal lunar (M_2) tide, which has frequency $\sigma \sim 1.4 \times 10^{-4}\,\mathrm{s}^{-1}$. The characteristic tidal wavelength is $L_g \sim 2\pi\sqrt{gH_0}/\sigma \sim 300\,\mathrm{km}$, where g is the acceleration due to gravity and a characteristic water depth $H_0 = 5\,\mathrm{m}$ is used. The spatial scales of the phenomena that are the focus of this study (typically $L_{\mathrm{barrier}} \sim 10\,\mathrm{km}$) are small compared to the wavelength of the tidal wave. Hence, the Froude number ($\mathrm{Fr} \sim L_{\mathrm{barrier}}/L_g$) is very small. This allows for a rigid lid approximation: the sea level variations themselves can be neglected, but their spatial gradients are important and result in pressure gradients in the momentum equations (see e.g., Calvete et al., 2001). The hydrodynamic equations are

$$\frac{\partial \vec{u}}{\partial t} + (\vec{u}\cdot\vec{\nabla})\vec{u} + f\vec{e}_z \times \vec{u} = -g\vec{\nabla}\zeta - \frac{\vec{\tau}_b}{\rho H}, \tag{1a}$$

$$\vec{\nabla}\cdot(H\vec{u}) = 0. \tag{1b}$$

Here, $\vec{u}$ is the horizontal velocity vector, t is time, $\vec{\nabla}$ the horizontal gradient operator, f the Coriolis parameter, $\vec{e}_z$ the unity vector in vertical direction, ζ the elevation of the free surface, H the water depth with respect to $z = 0$, $\vec{\tau}_b$ the bed shear-stress and ρ the density of water. Usually, the bed shear-stress is taken to depend quadratically on the local velocity. In this study a linearized bed shear-stress formulation is used:

$$\vec{\tau}_b = \rho r\vec{u}, \quad r = \frac{8}{3\pi}C_d U, \tag{2}$$

with $C_d \sim 0.0025$ the drag coefficient and U the mean tidal velocity amplitude at the transition line. The friction coefficient r is taken such that the tidally averaged dissipation of energy at the transition line due to the linearized bottom stress equals that of the quadratic bottom stress. A discussion on the derivation of the linearized bed shear-stress is given in Zimmerman (1992).

Currents in this model are forced by a prescribed alongshore pressure gradient. Periodic boundary conditions in the alongshore direction are imposed (with an as yet unspecified length scale). Furthermore, the shore-normal velocity component must vanish at the transition line and far offshore the velocity is assumed to have a vanishing cross-shore component (no exchange of water between inner shelf and nearshore zone),

$$u = v\frac{\partial x_{\mathrm{t}}}{\partial y} \text{ at } x = x_{\mathrm{t}}, \quad u \to 0 \text{ for } x \to \infty, \tag{3}$$

where u, v are the cross-shore and alongshore component of the velocity vector $\vec{u}$, respectively.

2.2. Alongshore volumetric sediment flux

The tidal hydrodynamics and sediment flux in the nearshore zone are not explicitly calculated in the model. Instead, the tidal currents are calculated on the inner shelf and the velocities at the transition line are taken as representative for the entire nearshore zone. They are used to calculate the volumetric flux of sediment q through an $x-z$-section across the nearshore zone (Fig. 2). This flux consists of two parts

$$q = q_{(\mathrm{wave})} + q_{(\mathrm{curr})}, \tag{4}$$

where $q_{(\mathrm{wave})}$ is the part due to waves only and $q_{(\mathrm{curr})}$ due to the joint action of tides and waves. It is assumed that $q_{(\mathrm{curr})}$ involves the stirring of sediment from the bed by waves, which is subsequently

transported by a tide-driven residual current. This is parameterized as

$$q_{(\mathrm{curr})} = \beta\langle v_{\parallel}\rangle. \tag{5}$$

Here, β is a constant and $\langle v_{\parallel}\rangle$ is the tidally averaged shore-parallel component of the velocity at the transition line:

$$\langle v_{\parallel}\rangle = \frac{1}{T}\int_0^{\mathrm{T}} v_{\parallel}\,\mathrm{d}t, \tag{6}$$

where T is the tidal period. The constant β in Eq. (5) accounts for the fact that the sediment is transported in the complete nearshore zone and has the unit m^2. A physical interpretation of β is the available volume of sediment in the nearshore zone per unit length:

$$\beta = \int_{x_c}^{x_t}\int_{-H}^{0} \frac{c}{\rho_s}\mathrm{d}z\,\mathrm{d}x. \tag{7}$$

In this expression c is the tidally averaged sediment mass concentration and ρ_s the density of the grains. The mean wave height along the Dutch and German Wadden coast is in the order of 1 m Sha (1989). Using observations performed by Grasmeijer and Kleinhans (2004) of sediment concentrations at different levels in the vertical in the nearshore zone near Egmond aan Zee (the Netherlands) yields an estimate of $\int(c/\rho)\,\mathrm{d}z = \mathcal{O}(5\times10^{-5}-1\times10^{-3})\,\mathrm{m}$. Assuming that the width of the nearshore zone is in the order of 500 m, this yields that $\beta = \mathcal{O}(0.05-0.5)\,\mathrm{m}^2$.

Finally, values of the alongshore sediment flux $q_{(\mathrm{wave})}$ are adopted from the model of Falqués (2006).

2.3. Evolution of the coastline

To obtain equations that govern the evolution of the coastline and the transition line we assume that the depth H_0 equals the average active water depth, which is defined in Falqués and Calvete (2005). Mass conservation of sediment then yields

$$\frac{\partial x_{\mathrm{t}}}{\partial t} = -\frac{1}{H_0}\frac{\partial q}{\partial y}. \tag{8}$$

Here, for simplicity, it is assumed that $(x_{\mathrm{t}} - x_{\mathrm{c}}) =$ constant.

Next, the magnitude of the morphological time scale T_m is estimated on which the coastline evolves due to alongshore variations in $q_{(\mathrm{curr})}$. From Eqs. (5) and (8) it follows:

$$\frac{[x_{\mathrm{t}}]}{T_m} = \frac{\beta[\langle v\rangle]}{H_0\lambda},$$

with $[x_{\mathrm{t}}]$ the cross-shore amplitude of the undulation of the coastline, λ its alongshore wavelength and $[\langle v\rangle]$ the magnitude of the residual current at the transition line (depth H_0). Typical values for the Dutch coast are $[x_{\mathrm{t}}]\sim500\,\mathrm{m}$, $\lambda\sim10\,\mathrm{km}$, $\beta\sim0.3\,\mathrm{m}^2$, $[\langle v\rangle]\sim0.05\,\mathrm{ms}^{-1}$ and $H_0 = 5\,\mathrm{m}$. Substitution of these values in the expression given above, the morphological time scale $T_m\sim50\,\mathrm{yr}$. Hence, the position of the coastline may be considered as constant during one tidal cycle.

3. Basic state and linear stability analysis

3.1. Basic state

The model solutions are denoted by vector $\Psi = (\vec{u}, \vec{\nabla}\zeta, x_{\mathrm{t}}, q_{(\mathrm{wave})})^{\mathrm{T}}$. This state vector can be split into a part which describes a basic state with alongshore uniform conditions and a part which describes deviations from this basic state, $\Psi = \Psi_{\mathrm{eq}} + \Psi'$. Here, $\Psi_{\mathrm{eq}} = (\vec{U}, \vec{\nabla}Z, X_{\mathrm{t}}, Q_{(\mathrm{wave})})^{\mathrm{T}}$ contains the basic state variables: $\vec{U} = (U, V)$ is the velocity vector with components U and V in the x- and y-direction, respectively, and $\vec{\nabla}Z$ is the gradient of the sea surface. Furthermore, $X_{\mathrm{t}} =$ constant is the position of the transition line in the basic state (straight coast) and $Q_{(\mathrm{wave})}$ is the undisturbed wave-driven sediment flux in the breaker zone.

In the basic state, a spatially uniform alongshore pressure gradient is prescribed that consists of a residual component (S_0) and the main tidal (M_2) component with amplitude S_2 and frequency σ,

$$\frac{\partial Z}{\partial y} = -S_2\cos\sigma t + S_0. \tag{9}$$

No higher harmonics of the tide are taken into account. The free surface elevation Z is linear in the alongshore direction. The velocity in the basic state has an alongshore component that varies only in the cross-shore direction, i.e., $\vec{U} = (0, V(x,t))$. This velocity component is determined by a balance between inertia, alongshore sea surface gradient and depth-dependent friction,

$$\frac{\partial V}{\partial t} = -g\frac{\partial Z}{\partial y} - r\frac{V}{H}. \tag{10}$$

The solution of this equation is

$$V(x,t) = V_2(x)\cos(\sigma t + \Phi(x)) + V_0(x), \tag{11}$$

with

$$V_2(x) = \frac{HS_2 g}{\sqrt{\sigma^2 H^2 + r^2}}, \quad \Phi(x) = \arctan\left(\frac{-\sigma H}{r}\right),$$

$$V_0(x) = \frac{-gS_0}{r} H. \tag{12}$$

The depth-dependent friction term in the alongshore momentum balance causes a phase lag between currents and sea surface gradient (in case of time dependent pressure gradient). It also results in an increasing magnitude of the alongshore velocity with increasing depth, i.e., cross-shore distance. Hence, the basic state velocity contains vorticity, defined by $\Omega(x,t) = \partial V(x,t)/\partial x$. Furthermore, a characteristic tidal velocity amplitude U is defined as

$$U = V_2(x = X_t). \tag{13}$$

Upon substitution of the basic state variables in Eq. (5) it follows that in the basic state the sediment flux due to currents reads

$$Q_{(\mathrm{curr})} = \beta V_0. \tag{14}$$

3.2. Stability analysis

The stability of the alongshore uniform coastline is studied by considering the dynamics of alongshore rhythmic perturbations. Hence, in Eqs. (1)–(8) $\Psi = \Psi_{\mathrm{eq}} + \Psi'$ is substituted, with Ψ_{eq} as defined in Eqs. (9), (11). Furthermore, $\Psi' = (\vec{u}', \vec{\nabla}\zeta', x_t', q'_{(\mathrm{wave})})^{\mathrm{T}}$ denotes the state vector with the perturbed variables. The magnitudes of the latter are assumed to be much smaller than those of the corresponding variables in the basic state.

Linearizing the equations of motion with respect to the small variables yields

$$\frac{\partial u'}{\partial t} + V\frac{\partial u'}{\partial y} - fv' = -g\frac{\partial \zeta'}{\partial x} - \frac{ru'}{H}, \tag{15a}$$

$$\frac{\partial v'}{\partial t} + \left(u'\frac{\partial V}{\partial x} + V\frac{\partial v'}{\partial y}\right) + fu' = -g\frac{\partial \zeta'}{\partial y} - \frac{rv'}{H}, \tag{15b}$$

$$u'\frac{\mathrm{d}H}{\mathrm{d}x} + H\frac{\partial u'}{\partial x} + H\frac{\partial v'}{\partial y} = 0. \tag{15c}$$

The linearized boundary conditions (3) are

$$u' = V\frac{\partial x_t'}{\partial y} \text{ at } x = X_t, \quad u' \to 0 \text{ for } x \to \infty. \tag{16}$$

The next step is to find the perturbed sediment fluxes $q'_{(\mathrm{curr})} \equiv q_{(\mathrm{curr})} - Q_{(\mathrm{curr})}$ and $q'_{(\mathrm{wave})} \equiv q_{(\mathrm{wave})} - Q_{(\mathrm{wave})}$. Using Eq. (5) and the definition $v_{\parallel} = \vec{u}\cdot\vec{s}$, with $\vec{s}$ the tangent vector at the transition line, the alongshore sediment flux due to the joint action of tides and waves reads

$$Q_{(\mathrm{curr})} + q'_{(\mathrm{curr})} = \left.\frac{\beta\langle V + v'\rangle}{[1 + (\partial x_t'/\partial y)^2]^{1/2}}\right|_{x = X_t + x_t'}. \tag{17}$$

Subsequently, a Taylor expansion of the various variables at $x = X_t$ is made and only contributions are kept that are linear in the perturbed quantities. Finally, using Eq. (14), the result is

$$q'_{(\mathrm{curr})} = \beta\left[\langle v'\rangle + x_t'\frac{\mathrm{d}\langle V_0\rangle}{\mathrm{d}x}\right]_{x = X_t}. \tag{18}$$

The values for the perturbed sediment flux $q'_{(\mathrm{wave})}$ are adopted from Falqués (2006). Finally, the linearized equation for the evolution of the transition line reads

$$\frac{\partial x_t'}{\partial t} = -\frac{\beta}{H_0}\frac{\partial}{\partial y}\left[\langle v'\rangle + x_t'\frac{\mathrm{d}}{\mathrm{d}x}\langle V_0\rangle\right]\Bigg|_{x = X_t} - \frac{1}{H_0}\frac{\partial q'_{(\mathrm{wave})}}{\partial y}. \tag{19}$$

Recall that in this model $x_t' = x_c'$, so Eq. (19) also governs the evolution of the perturbation of the coastline.

3.3. Solution procedure

The model equations have solutions of the form

$$\Psi' = \Re[(\hat{u}(x,t), \hat{v}(x,t), \hat{\vec{\nabla}}\hat{\zeta}(x,t), \hat{x}_t, \hat{q}_{\mathrm{wave}})\mathrm{e}^{\mathrm{i}ky}\mathrm{e}^{\Gamma t}]^{\mathrm{T}}, \tag{20}$$

where $\Re$ stands for taking the real part. Note that all variables behave exponentially in time. Besides, the flow variables also show oscillatory behavior on the tidal time scale which is much smaller than the time scale on which the transition line is evolving. The alongshore wave number is denoted by k and can be chosen arbitrarily. Furthermore, $\Gamma = \Gamma_{\mathrm{re}} + \mathrm{i}\Gamma_{\mathrm{im}}$ is the complex growth rate, with a real part (Γ_{re}) that describes the growth of the perturbations, and an imaginary part (Γ_{im}) that determines the phase speed, $c = -\Gamma_{\mathrm{im}}/k$.

The aim is to determine $\hat{u}(x,t), \hat{v}(x,t), \hat{\vec{\nabla}}\hat{\zeta}(x,t)$, $\hat{x}_t, \hat{q}_{\mathrm{wave}}$ and Γ as a function of wavenumber k and model parameters. The interest is in perturbations that have positive growth rates ($\Gamma_{\mathrm{re}} > 0$). The mode with wave number $k = k_p$ that has the largest growth rate will dominate the dynamics after some

time. Therefore, it is called the most preferred mode. The growth rate is calculated as follows. First, the perturbation x_t with given wave number k is chosen. The hydrodynamic problem, described by Eqs. (15a)–(15c) and boundary conditions (16), has to be solved. Because the alongshore dependence of the variables is known a priori, $\hat{v}$ is known as a function of $\hat{u}$ (Eq. (15c)), and reads

$$\hat{v} = -\frac{\hat{u}(\mathrm{d}H/\mathrm{d}x) + H(\partial\hat{u}/\partial x)}{\mathrm{i}kH}. \tag{21}$$

Next, a vorticity equation is derived by taking the x-derivative of the alongshore momentum equation (15b) and subtracting the y-derivative of Eq. (15a). When substituting for $\hat{v}$, one equation for the complex cross-shore velocity $\hat{u}$ is found:

$$U_{12}\frac{\partial^3\hat{u}}{\partial t\partial x^2} + U_{11}\frac{\partial^2\hat{u}}{\partial t\partial x} + U_{10}\frac{\partial\hat{u}}{\partial t} + U_{02}\frac{\partial^2\hat{u}}{\partial x^2} + U_{01}\frac{\partial\hat{u}}{\partial x} + U_{00}\hat{u} = 0. \tag{22}$$

The coefficients U_{ij} are identical to those given in Calvete et al. (2001). In this problem one boundary condition is different, viz. at $x = X_t$ variable $\hat{u}$ is prescribed. Furthermore, for $x \to \infty$ it is required that $\hat{u} \to 0$. Solving Eq. (22) together with the boundary conditions yields $\hat{u}$, and using Eq. (21) yields $\hat{v}$. Substituting Eq. (20) into Eq. (19) yields an expression for growth rate Γ:

$$\Gamma\hat{x}_t = -\frac{\beta}{H}\left(\mathrm{i}k\langle\hat{v}\rangle + \mathrm{i}k\hat{x}_t\frac{\mathrm{d}V_0}{\mathrm{d}x}\right)\bigg|_{x=X_t} - \frac{\mathrm{i}k\hat{q}_{\mathrm{wave}}}{H}. \tag{23}$$

3.4. Numerical implementation

Eq. (22) is solved using a pseudospectral method. The spatial variables are expanded in Chebyshev polynomials (see Boyd, 2001 for details). In previous morphodynamic modeling studies these Chebyshev polynomials have been successfully used in resolving spatial patterns (Falqués et al., 1996). Employing the method discussed in Calvete et al. (2001), for the time-dependent part a Galerkin approach is adopted. The velocity component $\hat{u}$ and $\hat{v}$ are expanded in their harmonic agents M_0, M_2, M_4 and so on. In this study the series is truncated after the M_2 components, so nonlinear tides are not accounted for. Hence, the cross-shore velocity component is expanded as

$$\hat{u}(x,t) = \sum_{j=0}^{N-1}[u_j^0 + u_j^{-1}\mathrm{e}^{-\mathrm{i}\sigma t} + u_j^1\mathrm{e}^{\mathrm{i}\sigma t}]T_j(\tilde{x}) \tag{24}$$

and a similar expansion for $\hat{v}$ is used. In the expression above, $x = L_x(1+\tilde{x})/(1-\tilde{x})$ with L_x a stretching parameter and T_j are Chebyshev polynomials. Furthermore, N is the number of collocation points in the x-direction and u_j^0, u_j^{-1}, u_j^1 are the Chebyshev coefficients of the residual component, the $\mathrm{e}^{-\mathrm{i}\sigma t}$ Fourier component and the $\mathrm{e}^{\mathrm{i}\sigma t}$ Fourier component of the cross-shore velocity, respectively. The expansion (24) is substituted into Eq. (22) and is evaluated at N collocation points in the x-direction. This results in a system of $3N$ by $3N$ linear algebraic equations with $3N$ variables of the form $A\chi = B$, which is solved by standard numerical techniques. Here, A is a complex $3N$ by $3N$ matrix describing the model equations. The vector χ contains the coefficients of the expansions of Eq. (24). The $3N$ elements of complex vector B are all zero, except those which are linked to values of $\hat{u}$ at the collocation point which represents the transition line. At that location $\hat{u}$ is prescribed (boundary condition (16)).

4. Results

4.1. Reference case

The focus of this study is on the influence of tidal currents on the stability of the equilibrium state with respect to perturbations in the position of the coastline. Thus, $q'_{(\mathrm{wave})} = 0$ is assumed in Eqs. (19), implying that $\hat{q}_{\mathrm{wave}} = 0$ in Eq. (23). Experiments are performed for parameter values which are representative for the Dutch coastal area. The following profile has been used to represent the depth profile of the inner shelf:

$$H(x) = H_0 + (H_s - H_0)(1 - \mathrm{e}^{-(x-X_t)/L}). \tag{25}$$

Here, $H_0 = H(x = x_t)$ and far offshore, where the inner shelf connects to the outer shelf, the depth is H_s. Parameter L is an e-folding length scale which is a measure of the width of the inner shelf. Typical values have been determined by fitting this expression to observed profiles along the Dutch coast (Fig. 3). This yields estimates of $H_0 \sim \mathcal{O}(1-10)\,\mathrm{m}$, $H_s \sim \mathcal{O}(15-25)\,\mathrm{m}$ and $L \sim \mathcal{O}(8-15)\,\mathrm{km}$. In the reference experiment $H_0 = 5\,\mathrm{m}$, $H_s = 20\,\mathrm{m}$ and $L = 10\,\mathrm{km}$. The alongshore sea surface gradient is chosen such that the tidal velocity amplitude at the transition line is $U = 0.5\,\mathrm{ms}^{-1}$. No net flow is considered in the basic state ($S_0 = 0$). The Coriolis parameter is $f = 1.14 \times 10^{-4}\,\mathrm{s}^{-1}$, the drag coefficient $C_d = 2.5 \times 10^{-3}$ and $\beta = 0.3\,\mathrm{m}^2$. The number

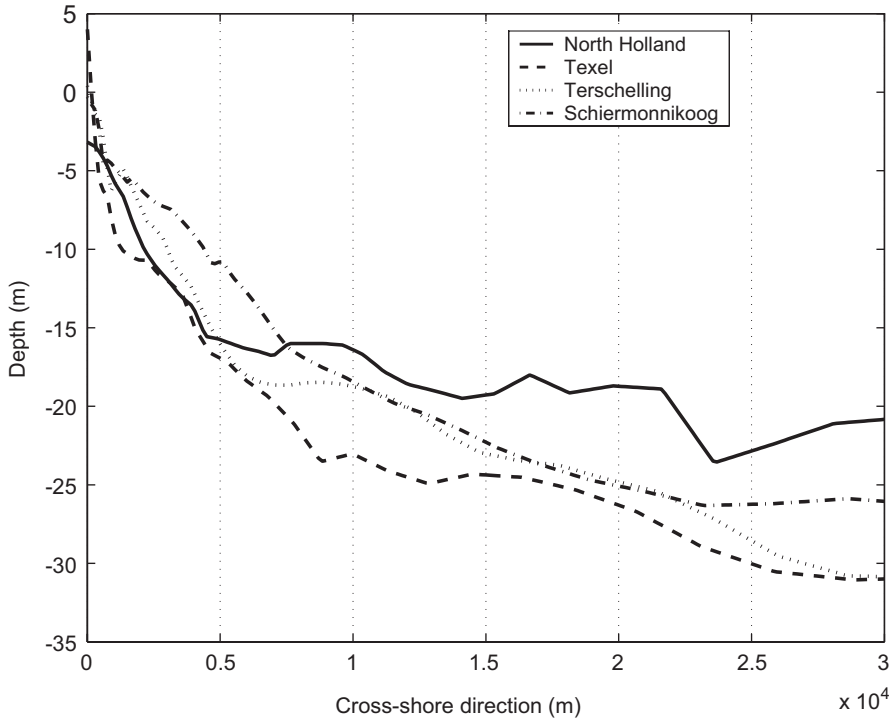

Fig. 3. Four cross-shore profiles along the Dutch coast. The profile of 'North Holland' was measured 20 km south of Den Helder. The locations of Texel, Terschelling and Schiermonnikoog can be found on Fig. 1.

of collocation points is $N = 100$ and the stretching parameter $L_x = 10\,\mathrm{km}$.

The dependence of the growth rate on the alongshore wave number is shown in the top panel of Fig. 4. The growth rate has been made dimensionless such that a value of 1 corresponds to an e-folding time scale of 50 yr. The variable along the horizontal axis is the non-dimensional alongshore wave number $kL = 2\pi L/\lambda$, where λ is the wavelength and $L = 10\,\mathrm{km}$ is the width of the inner shelf. The basic state is stable with respect to perturbations having small values of the dimensionless wave number, corresponding to wavelengths which are long compared to the width of the inner shelf. Perturbations with these wavelengths have negative growth rates and hence decay exponentially. For $kL > 3$ the growth rate increases with increasing kL and for $kL \sim 8.2$ the growth rate is zero. The wavelength of the perturbation with zero growth rate is called λ_0. In this case $\lambda_0 = 7.6\,\mathrm{km}$. For $kL > 8.2$ the growth rate is positive. Hence, there is a positive feedback between the coastline perturbation and the tidal flow. The growth rate curve does not show a maximum, so there is no fastest growing mode (FGM).

The model also yields the phase speed of the perturbations. This phase speed is shown as a function of the dimensionless alongshore wave number in the bottom panel of Fig. 4. It has a minimum for $kL \sim 8$ and increases for larger kL. A nondimensional phase speed of -0.1 is in dimensional values $-20\,\mathrm{m/yr}$. A negative sign means that the perturbation is migrating in the negative y-direction, that is to the right when viewing in the seaward direction.

The perturbed sediment flux $q'_{(\mathrm{curr})}$ is linear in the residual currents (Eq. (18)). The left panel of Fig. 5 shows a vector plot of the residual currents on the inner shelf. Because the model does not yield a FGM, a wavelength is chosen that has a positive growth rate, $\lambda = 3\,\mathrm{km}$ ($kL = 20.9$). Furthermore, because the model is linear in x'_t an amplitude is chosen of $[x'_t] = 500\,\mathrm{m}$. Two residual circulation cells per alongshore wavelength appear. In this case the typical magnitude of the residual currents is $0.01\,\mathrm{ms}^{-1}$. The structure of the residual circulation cells is such that the maximum convergence of the velocity at the transition line (and hence the convergence of the net sediment flux) is slightly out of phase (to the right when viewing in the

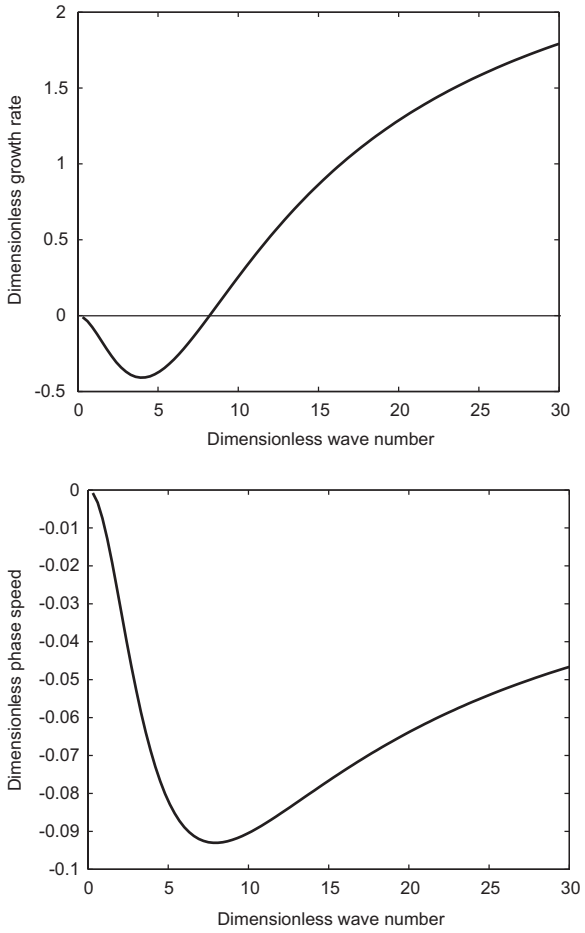

Fig. 4. Top: growth rate as function of wave number for the reference case. A growth rate of 1 corresponds to an *e*-folding time scale of 50 yr. Wave numbers are scaled with the width of the inner shelf, 10 km. Bottom: phase speed as a function of wave number for the reference case. A phase speed of −0.1 corresponds to a dimensional phase speed of −20 m/yr.

seaward direction) with the coastline perturbation. The perturbation will therefore grow and migrate. The migration is forced by the Coriolis force. When $f = 0$, there is no phase difference between the residual velocities at the transition line and the coastline perturbation (right panel of Fig. 5). Hence, the perturbation does not migrate.

4.2. Sensitivity of results to tidal current amplitude

Observations show that the shore-parallel tidal current amplitudes on the transition line vary between approximately 0.1 and $\sim$1 ms^{-1} in regions where barrier islands are observed. In the reference case the tidal velocity amplitude at the transition line was 0.5 ms^{-1}. In the next experiment the magnitude of the basic state tidal velocity at the transition line is varied between 0.1 and 1.0 ms^{-1}. A change in the magnitude of the basic state velocity causes a change of the magnitude of the friction parameter r, defined in Eq. (2). The friction parameter scales linearly in the magnitude of the tidal velocity. All other parameters have the same value as in the reference experiment.

The influence of the magnitude of the tidal currents at the transition line (U) on the growth rate is shown in the top panel of Fig. 6. Larger values of U result in larger growth rates for large kL. Furthermore, a larger velocity magnitude results in a larger λ_0. Hence, coastline perturbations with larger length scales grow exponentially in time. For $U = 0.1\,\mathrm{ms}^{-1}$ $\lambda_0 = 4.5$ km, while for $U = 1\,\mathrm{ms}^{-1}$ $\lambda_0 = 10.3$ km.

A change of the magnitude of the tidal currents at the transition line (U) leads to only a moderate change of the phase speed (bottom panel of Fig. 6). The plot reveals that a change in U will not influence the phase speed of the coastline perturbation for small wavelengths. For larger wavelengths the tidal current amplitude does influence the phase speed. A smaller tidal current results in a smaller phase speed. However, a doubling of the tidal current amplitude with respect to the reference experiment hardly affects the phase speed for small kL.

In the next experiment, a time-invariant pressure gradient S_0 is prescribed. Hence, the basic state velocity has a residual component on top of the tidal component. Its profile is described by Eq. (12). The residual pressure gradient is chosen such that $V_0(x = X_t)$ is varied between 0.02 and $-0.02\,\mathrm{ms}^{-1}$. This implies that the residual currents far offshore are varied between -0.1 and $0.1\,\mathrm{ms}^{-1}$ for the reference bathymetry. All other parameters have their reference values. Results (not shown) indicate that only the phase speeds, not the growth rates, of perturbations of the coastline are strongly affected by this basic state residual current. For $V_0(x = X_t) = -0.02\,\mathrm{ms}^{-1}$ all perturbations are migrating to the right (when viewing in seaward direction). For smaller wavelengths (larger kL) the phase speed is larger. For $V_0(x = X_t) = 0.02\,\mathrm{ms}^{-1}$ the perturbations are all migrating to the right.

4.3. Sensitivity of results to bathymetric parameters

The bathymetry of the inner shelf influences the basic state velocity profile. In this section the

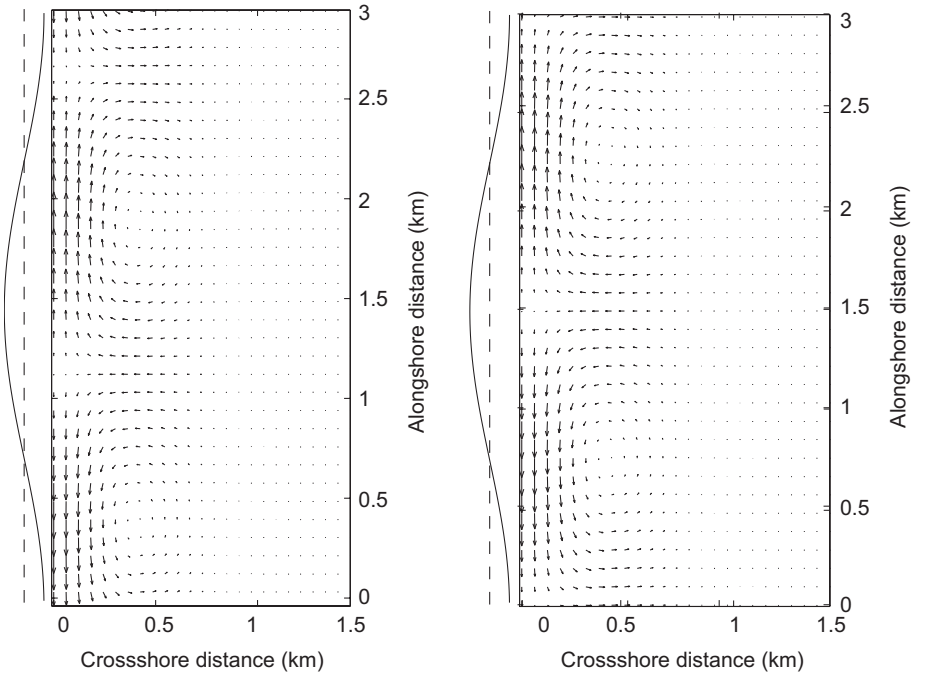

Fig. 5. Top: vector plot of residual currents for a perturbation of the coastline with alongshore wavelength $\lambda = 3$ km; reference case. The coastline perturbation is shown at the left-hand side. An amplitude of the coastline perturbation of $[x_t'] = 500$ m has been chosen. This yields that $[\langle u' \rangle] \sim [\langle v' \rangle] = 10^{-2}\,\mathrm{ms}^{-1}$. The residual flow is such that the perturbation is amplified. In addition, the Coriolis force induces a migration of the perturbation. Bottom: same as top panel, but now the residual currents in the case of no Coriolis. In this case the coastline perturbation only grows and is not migrating.

sensitivity of the results to the bathymetric parameters L and H_0 is studied. First, the length of the inner shelf is varied with all other parameters having their reference values. Results (not shown) reveal that a steeper profile results in smaller values of the wavelength of the perturbation with zero growth rate λ_0. The dependence of λ_0 on L is almost linear: $\lambda_0 \sim 3.8$ km for $L = 5$ km and $\lambda_0 \sim 12.3$ km for $L = 20$ km. Not only λ_0 changes, but also the growth rate. For small values of L, growth rates are larger for small wavelengths compared to the reference case. For relatively large values of L, growth rates are smaller for small wavelengths compared to the reference case. For a fixed wavenumber k the magnitude of the phase speed increases with decreasing L. For $L = 5$ km the phase speed has a maximum of 32 m/yr for $\lambda = 6.8$ km ($kL = 9$).

Next, the dependence of the results on the value of H_0 is investigated. When H_0 is changed the value of β has to be changed as well. Parameter β can be interpreted as the volume per unit length in the alongshore direction of sediment that is in suspension in the nearshore zone (see Eq. (7)). It is assumed that the steepness of the nearshore zone is constant and that the average concentration in the nearshore zone does not change with changing H_0. From this it follows that $\beta \sim H_0^2$. Furthermore, when H_0 is changed and the alongshore sea surface gradient S_2 is kept fixed the magnitude of the bottom friction coefficient r should be changed as well. However, it is assumed that the profile of the basic state velocity is not changed, which implies that the velocity profile is such that the tidal current amplitude is $0.5\,\mathrm{ms}^{-1}$ at 5 m depth. The friction coefficient r and the amplitude of the M_2 pressure gradient S_2 keep their reference values.

The results of Fig. 7 show that a smaller H_0 results in a shift of λ_0 to smaller wavelengths. For small wavelengths a smaller H_0 results in larger growth rates, compared to the reference case (top panel of Fig. 7). The influence of H_0 on the phase speed is shown in the bottom panel of Fig. 7. An increase of H_0 with respect to the reference experiment results in an increase of the phase speed. A decrease of H_0 results in a decrease of the phase speed.

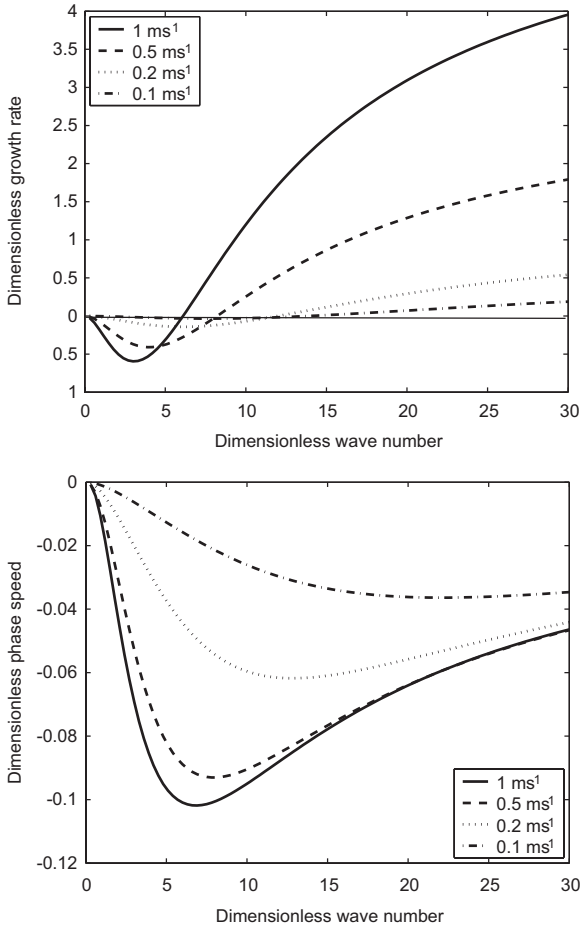

Fig. 6. Top: Growth rate curves for different values of the magnitude of the basic state tidal M_2 flow at the transition line. The magnitude of U is 0.1, 0.2, 0.5 and 1.0 ms^{-1}, respectively. A dimensionless growth rate of 1 corresponds to time scale of 50 yr and alongshore wave number is scaled with 10 km. Bottom: same as top panel, but now the phase speed as a function of the wave number. A non-dimensional phase speed of -0.1 is in dimensional values -20 m/yr.

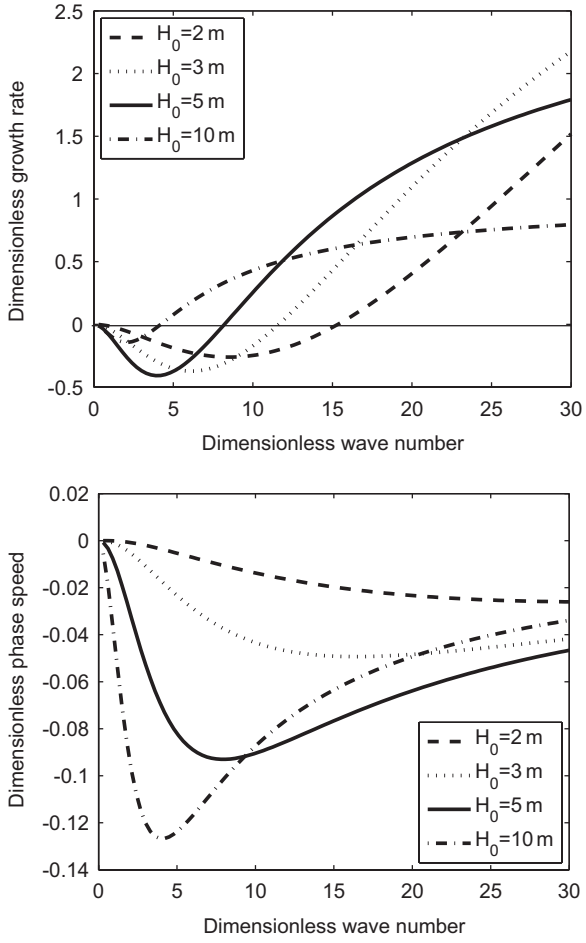

Fig. 7. Top: growth rate curves for different values of H_0. A dimensionless growth rate of 1 corresponds to time scale of 50 yr and alongshore wave number is scaled with 10 km. Bottom: Same as top panel, but now the phase speed as a function of the wave number. A dimensionless phase speed of -0.1 is in dimensional values -20 m/yr.

4.4. Influence of waves on the instability mechanism

In all the previous experiments, i.e. with significant tidal currents and $q_{(\mathrm{wave})} = 0$, no FGM was obtained. Hence, the model cannot explain why undulations of the coastline have preferred length scales, as field data indicate. Furthermore, the growth rates are largest for the smallest wavelengths, which implies that perturbations with an infinitesimal small length scale will grow fastest. Hence, the model is missing a mechanism that results in decay of the perturbations with the smallest length scale. The results of Falqués (2003), Falqués and Calvete (2005) indicate that when a net volumetric sand flux due to obliquely incident waves ($q'_{(\mathrm{wave})}$) is accounted for, a selection mechanism for the growing perturbations is introduced.

Results of the full eigenvalue problem (23) were computed for three different sectors of the Dutch coast: the southern delta coast, the central Holland coast and the northern Wadden coast. For the tidal model all parameters have their reference value, except that a value of $H_0 = 9$ m has been used, which is consistent with the value that has been used in Falqués (2006). Recall that β scales quadratically in the value of H_0. Values for the perturbed wave flux $q'_{(\mathrm{wave})}$ were adopted from Falqués (2006). Note that in the latter study different shape functions of

topographic variations induced by undulations of the coastline are assumed than in the present flow model. This means that results only give a first indication of the effect of the sediment fluxes $q_{(curr)}$ and $q_{(wave)}$ on the characteristics of undulations of the coastline.

In the top panel of Fig. 8 the growth rate curves and migration curves are shown for the northern Wadden coast. The solid curves represent the solutions of the full eigenvalue problem. Here the values of case C of Falqués (2006) are used, for which the topographic shape function has a local maximum at 300 m from the coast. It has been selected because this shape function results in the largest growth rates due to waves only. When using other shape functions growth rates were negative for all wavelengths and waves damp the instability mechanism due to tides. It appears that without tides there is a preferred mode with has the largest growth rate, but it grows very slowly (*e*-folding time scale is about 50 yr). Furthermore, also the perturbations of the coastline with very long wavelengths can grow. When tides are accounted for the scale selection becomes more pronounced: the growth rates of long waves becomes negative and the maximum growth rate increases by approximately 50%. Thus, it seems that tides enhance the instability of the northern Dutch coast. Furthermore, the wave number of the preferred mode shifts to larger values (the preferred wavelength reduces from 7.8 km to about 7.5 km). The migration speeds of the perturbations slightly increase with respect to the case that only a wave flux is considered and are in the order of 200 m/yr.

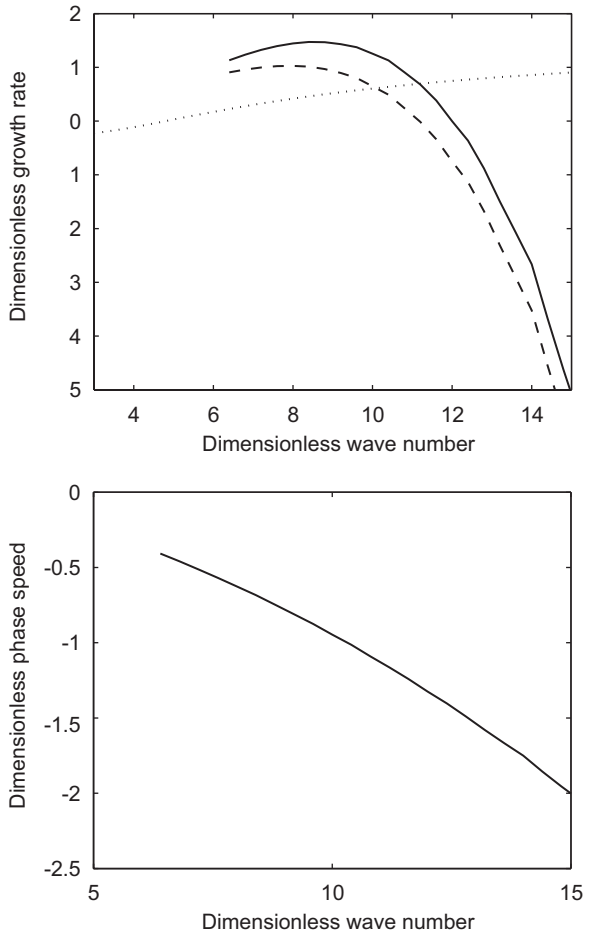

Fig. 8. Top: dimensionless growth rate Γ_r versus dimensionless longshore wavenumber k as calculated with the combined wave–tide model for the northern Dutch coast (solid line). Parameters of the tidal model have their default values, except that $H_0 = 9$ m (results shown by dotted line); for the wave model the data of Falqués (2006) for case C are adopted (results shown by dashed line). A value $\Gamma_r = 1$ corresponds to an *e*-folding time scale of 50 yr. Bottom: as top panel, but dimensionless migration speed c versus k. A value $c = 0.1$ corresponds to a speed of 20 myr^{-1}.

Sensitivity experiments show that the wavelength of the preferred mode is a function of the magnitude of tidal currents at the transition line (Fig. 9). When $U = 0.1\,\mathrm{ms}^{-1}$ the preferred wavelength is 7.85 km, while for $U = 0.8\,\mathrm{ms}^{-1}$ the preferred wavelength is 7.15 km. Hence, the model results predict that the wave length of the preferred mode decreases with increasing magnitude of the tidal currents.

The model has also been applied to the central Holland coast and the southern delta coast (results

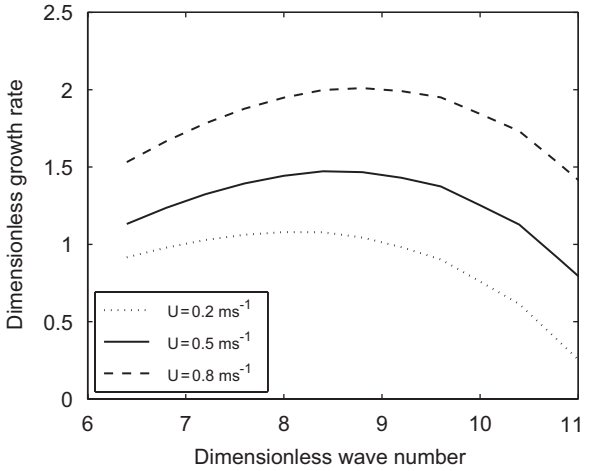

Fig. 9. Growth rate curves calculated with the combined wave–tide model for different values of tidal current amplitude at sea. Other parameters have their default values for the Dutch and German Wadden coast.

not shown). For the latter case the effects of tides on the dynamics of undulations of the coastline are not so large and waves overwhelm the positive feedback mechanism due to tides. For the Holland coast tides only have a marginal effect on the dynamics of the undulations of the coastline in case profile A, C or D (Falqués, 2006) is chosen. However, if a different topographic shape factor is selected (case B of Falqués, 2006) tides cause positive growth rates for wave lengths larger than 9.5 km when $U = 0.7\,\mathrm{ms}^{-1}$. Because no data is available of the wave model of Falqués (2006) for wave lengths larger than 10 km the presence of a FGM could not be studied.

5. Physical interpretation

It was shown that for the default settings of the model parameters, perturbations with wavelengths $\lambda > 8$ km have negative growth rates, while for $\lambda < 8$ km the growth rate is positive. The perturbations not only grow but also migrate to the right when viewing in the seaward direction. When wave effects are included in the calculation of the alongshore sediment flux, a fastest growing mode is obtained. In this section these results are explained in terms of basic physical mechanisms. The emphasis is on the role of tides in this mechanism. The influence of wave-induced alongshore sediment fluxes on the evolution of perturbations of the coastline has already been discussed in Falqués and Calvete (2005).

The growth and migration of the perturbations are due to the divergence of the volumetric sediment flux $q'_{(\mathrm{curr})}$ as defined in Eq. (18). This flux is linearly related to the tidally averaged velocity at the transition line, which is related to circulation patterns (see Fig. 5) on the inner shelf. The physics causing the generation of residual circulation cells will be analyzed using vorticity concepts in a similar way as described in Zimmerman (1981). The vorticity balance for the perturbed variables, retaining only linear terms, is obtained by taking the x-derivative of Eq. (15b) and subtracting the y-derivative of Eq. (15a),

$$\overbrace{\frac{\partial \omega'}{\partial t}}^{(a)} + \overbrace{\frac{\partial (u'\Omega)}{\partial x}}^{(b)} + \overbrace{\frac{\partial}{\partial y}(V\omega' + v'\Omega)}^{(c)} - \overbrace{\frac{r}{H^2}\frac{\mathrm{d}H}{\mathrm{d}x}v'}^{(d)} + \overbrace{f\left(\frac{\partial u'}{\partial x} + \frac{\partial v'}{\partial y}\right)}^{(e)} = \overbrace{\frac{-r\omega'}{H}}^{(f)}. \tag{26}$$

Here, $\Omega = \partial V/\partial x$ is the vorticity of the basic state flow and $\omega' = \partial v'/\partial x - \partial u'/\partial y$ is the vorticity of the perturbed flow. In Eq. (26), term (a) models the local time evolution of the perturbed vorticity, term (b) the cross-shore gradient of the perturbed vorticity flux in the cross-shore direction, term (c) the alongshore gradient of the perturbed vorticity flux in the alongshore direction, term (d) the generation of perturbed vorticity by the frictional torque, term (e) the generation of perturbed vorticity due to vortex stretching of the planetary vorticity and term (f) the dissipation of perturbed vorticity due to bottom friction.

The model results reveal that the residual currents are organized in cells with cyclonic (anticyclonic) circulation. These cells are areas where the tidally averaged perturbed vorticity is positive (negative). To obtain the relation between the perturbation of the coastline and residual current at the transition line, it is thus important to study the tidally averaged vorticity balance. The latter follows from averaging Eq. (26) over the tidal period and reads

$$\overbrace{-\left[\frac{\partial}{\partial x}\langle u'\Omega\rangle + \frac{\partial}{\partial y}\langle V\omega' + v'\Omega\rangle\right]}^{(1)} + \overbrace{\frac{r}{H^2}\frac{\mathrm{d}H}{\mathrm{d}x}\langle v'\rangle}^{(2)} + \overbrace{\frac{f}{H}\frac{\mathrm{d}H}{\mathrm{d}x}\langle u'\rangle}^{(3)} = \overbrace{\frac{r}{H}\langle \omega'\rangle}^{(4)}. \tag{27}$$

Here, $\langle\,\rangle$ denotes an average over the tidal cycle, see Eq. (6) for its definition. Also, the continuity equation (15c) has been applied here. The three source terms of tidally averaged vorticity are on the left-hand side of Eq. (27). Term (1) describes the convergence of the tidally averaged perturbed vorticity flux, (2) the frictional torque due to alongshore currents over cross-shore sloping bathymetry and (3) the Coriolis torque due to vortex stretching. The right-hand side of Eq. (27), term (4), describes the dissipation of residual perturbed vorticity due to bottom friction.

Now, the different terms are estimated for a typical coastline perturbation of $\lambda = 3$ km, tidal currents at the transition line with a magnitude of $U = 0.5\,\mathrm{ms}^{-1}$, absence of residual currents at sea ($V_0 = 0\,\mathrm{ms}^{-1}$) and $f = 0$. The perturbation was already shown in Fig. 5. It turns out that in this case the magnitude of term (2) is much smaller than that of term (1) because the generated residual currents are much smaller than the M_2 component of u' and v'. The main balance in Eq. (27) is between the

production of tidally averaged perturbed vorticity described by term (1) and the dissipation of it described by term (4).

So, to understand the generation of residual circulation cells the focus should be on term (1), which describes the gradient of three fluxes of vorticity: $\langle u'\Omega\rangle$ is the mean flux of basic state vorticity by the perturbed cross-shore currents. The second one is $\langle\omega' V\rangle$ and represents the mean flux of perturbed vorticity by the basic state alongshore currents. The third one is $\langle v'\Omega\rangle$ and describes the mean flux of basic state vorticity by the perturbed alongshore currents.

First, consider the cross-shore gradient of $\langle u'\Omega\rangle$. During flood the basic state tidal currents are in the negative y-direction: V_2 is negative, see left panel of Fig. 10. Furthermore, $\partial V_2/\partial x<0$ and therefore $\Omega<0$. The perturbed cross-shore velocity u' during flood is 180° out of phase with the alongshore gradient of the coastline perturbation (left panel of Fig. 10, which shows the perturbed velocity vector $\vec{u}'$). The vorticity flux $u'\Omega$ is therefore in phase with the alongshore gradient of the coastline perturbation. Because the magnitude of $u'\Omega$ is decreasing in the cross-shore direction, the cross-shore gradient of $u'\Omega$ during flood results in areas on the inner shelf where vorticity is accumulating with a same sign as that of the alongshore gradient of the coastline perturbation. During ebb the value of V_2, Ω and u' change sign. This results in the same sign of $u'\Omega$ and in the same cross-shore gradient of $u'\Omega$. Hence, the cross-shore gradient of the mean cross-shore vorticity flux results in areas on the inner shelf characterized by mean perturbed vorticity which has the same sign as that of the alongshore gradient in the coastline perturbation. In other words, residual circulation cells as sketched in the middle panel of Fig. 10 are generated. The mean currents transport the sediment from areas where the coastline has accreted to areas where the coastline has eroded. This results in a decay of the perturbation of the coastline.

Next, consider the alongshore gradient of $\langle v'\Omega\rangle$ and $\langle V\omega'\rangle$. During flood $V_2<0$ and $\Omega<0$ (see above) and the perturbed alongshore velocity v' is 180° out of phase with the coastline perturbation (left panel of Fig. 10). The perturbed vorticity flux is $v'\Omega$ is therefore in phase with the coastline perturbation. The alongshore gradient of $v'\Omega$ is 180° out of phase with the alongshore gradient in the coastline perturbation and therefore leads to accumulation of vorticity with a sign that is opposite to that of the gradient of the coastline perturbation. In this case the residual circulation cells are as sketched in the right panel of Fig. 10. During ebb V_2, Ω and v' change sign. This results in

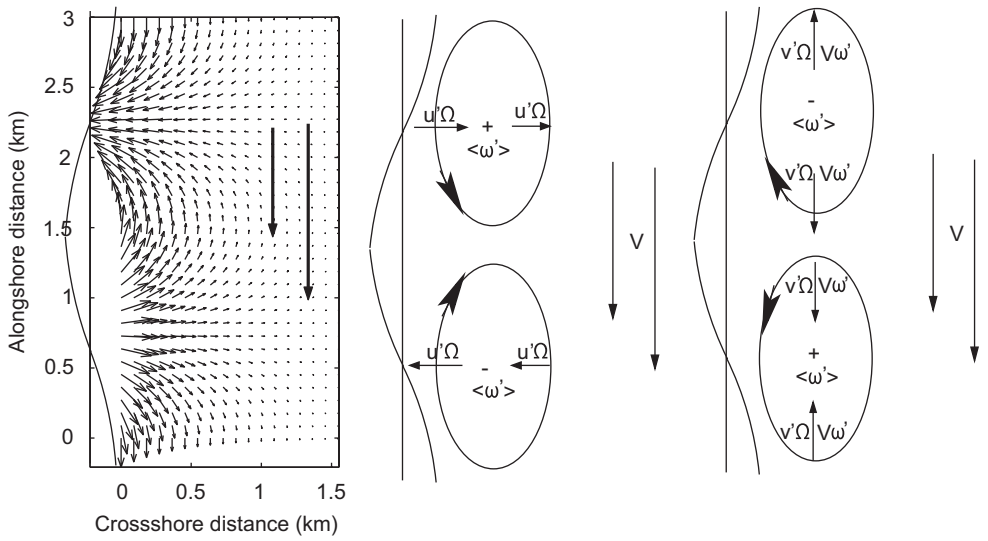

Fig. 10. Left: perturbed velocity induced by coastline at maximum flood. The basic tidal flow is from north to south (big arrows). The coastline perturbation has a cosine structure. Middle: small arrows represent perturbed cross-shore vorticity flux $u'\Omega$. The cross-shore gradient of the vorticity in the cross-shore direction generates two residual circulation cells (denoted by the two counter rotating cells) that cause a decay of the coastline perturbation. Right: same as middle panel, but now the alongshore gradient of the alongshore vorticity flux is visualized. Small arrows represent perturbed alongshore vorticity flux $v'\Omega$ and $V\omega'$. The alongshore gradient of the alongshore vorticity flux generates residual circulation cells that cause a growth of the coastline perturbation.

the same sign of $v'\Omega$ and in the same alongshore gradient of $v'\Omega$. Hence, averaged over one tidal cycle the alongshore gradient of $v'\Omega$ results in mean perturbed vorticity with a sign opposite to that of the alongshore gradient in the coastline perturbation. The mean currents transport the sediment from areas where the coast erodes to areas where the coast progrades. This causes the perturbation of the coastline to grow.

The last contribution to the convergence of the mean vorticity flux is the alongshore gradient of $\langle V\omega'\rangle$. During flood, the perturbed vorticity ω' is in phase with the coastline perturbation of the coastline and the perturbed vorticity flux is 180° out of phase with the coastline perturbation because $V_2<0$. Hence, following a similar argumentation as for the alongshore gradient of $\langle v'\Omega\rangle$, the alongshore gradient of $\langle V\omega'\rangle$ results in residual circulation cells that cause a growth of the perturbation of the coastline.

Whether the residual circulation cells are located along the coast in such a way that the coastline perturbation is growing or decaying depends on the magnitudes of the cross-shore gradient of $\langle u'\Omega\rangle$ and of the alongshore gradient of $\langle v'\Omega\rangle$ and $\langle V\omega'\rangle$. For small wave numbers the magnitude of the cross-shore gradient of $\langle u'\Omega\rangle$ is larger than the alongshore gradient of $\langle v'\Omega\rangle+\langle V\omega'\rangle$ and therefore the locations of the residual circulation cells are such that the perturbations of the coastline decay. For increasing wave numbers the magnitude of the alongshore gradient of $\langle v'\Omega\rangle$ and $\langle V\omega'\rangle$ increases stronger than that of the cross-shore gradient of $\langle u'\Omega\rangle$. When the magnitude of the alongshore gradient of $\langle v'\Omega\rangle+\langle V\omega'\rangle$ is larger than the cross-shore gradient of $\langle u'\Omega\rangle$, the locations of the generated residual circulation cells along the coast are such that the perturbations of the coastline grow.

When the Coriolis force is nonzero ($f\neq0$) the perturbations also migrate. The Coriolis torque (term (e) in Eq. (26)) is a source of tidal vorticity and causes a phase shift of the tidal vorticity with respect to the coastline perturbation. While in the case that $f=0$ the perturbed vorticity ω' is in phase with the coastline perturbation during flood, in the case that $f\neq0$ the maximum of the perturbed vorticity ω' is shifted in the negative y-direction with respect to the coastline perturbation due to planetary vortex stretching. The perturbed vorticity is transferred by the basic state velocity and the alongshore gradient of $V\omega'$ results in the accumulation of perturbed vorticity which is slightly shifted in the negative y-direction compared to the case that $f=0$. During ebb a similar argumentation holds and consequently, residual circulation cells occur of which the centers are shifted in the negative y-direction compared to those obtained in the case that $f=0$. Hence, the residual circulation cells in the case that $f\neq0$ cause both growth and migration of the coastline perturbation.

6. Discussion

In this section the results of the combined wave–tide model are compared with field data of undulations of bathymetric contours along the Dutch coast. Falqués (2006) already showed that his wave model yields wavelengths and migration speeds of the FGM that are consistent with those of observed shoreline sand waves along the southern and central Dutch coast. However, his model only yields very small growth rates when applied to the northern Wadden coast. It was shown in Section 4 that in this area the effect of tides on the initial formation of undulations of bathymetric contours is significant, hence we focus on this area.

Note that the present model only describes locations along the barrier where initially the coast tends to be more subject to erosion. It is hypothesized that during a severe storm at these locations channels are cut through the barrier and inlets form. An important finding of the model is that the length scale of the FGM decreases with increasing magnitude of the tidal currents U, and all other variables being constant. The predicted migration rates are in the order of $200\,\mathrm{myr}^{-1}$, depending on the specific parameter values, and perturbations are migrating to the east. To test the validity of these results observed lengths of barrier islands as well as wave and tidal characteristics along the Dutch and German Wadden coast were analyzed.

The length of the barrier islands along this coast varies between a few kilometers (Simonszand and Rottumeroog) up to 30 km (Texel) (Ehlers, 1988; Oost and de Boer, 1994). The typical migration speed of the islands is in the order of tens of meters per year and migration is from west to east (Luck, 1975). According to Sha (1989) the wave climate is almost constant in this area. Unfortunately, there are not many observations of the magnitude of the alongshore tidal currents at sea. Instead, the results of a numerical model were used. This is the ZUNO model from WL—Delft Hydraulics (Roelvink et al.,

2001), a model that has been developed to predict tidal heights and depth-averaged tidal currents in the southern North Sea. Fig. 11 shows the major axis of the M_2 tidal current ellipse in the region of the Frisian Islands. In the regions close to the tidal inlets currents are strongly influenced by the interaction between the backbarrier basin and the ebb-tidal delta. Therefore, the magnitudes of the major axis far offshore are considered. It is assumed that these are representative for the situation that the coastline is straight and no tidal inlets are present. Two transects (see the two lines in the top panel of Fig. 11) of the major axis of the M_2 tidal current ellipse are shown in the bottom panel of Fig. 11. These transects show that the long axis increases from Texel to Schiermonnikoog, where it attains a maximum, after which it decreases up to the island of Spiekeroog. The length of the barrier islands in this region is slightly larger than it is in the region just after Schiermonnikoog. These data seem to confirm our model prediction that the length scale of the barrier islands is inversely related to the magnitude of the shore-parallel tidal currents.

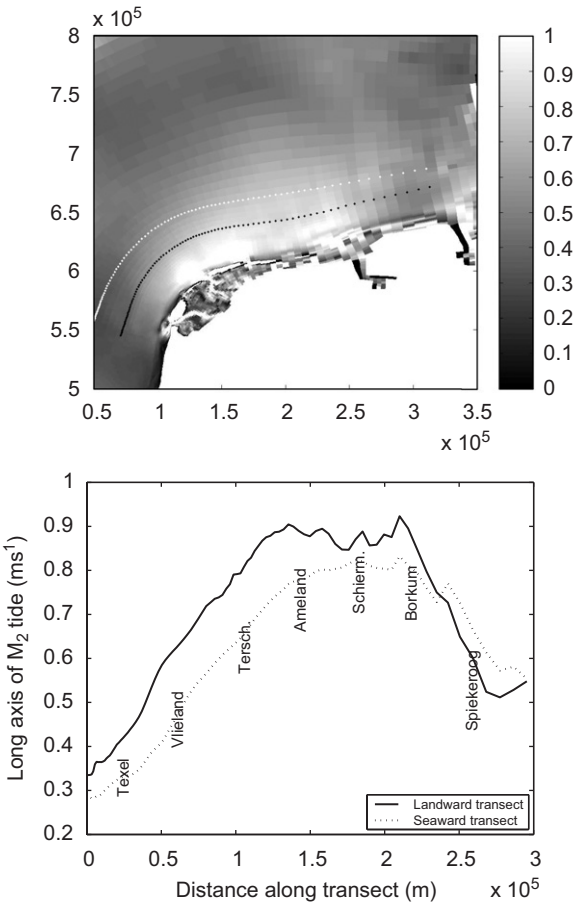

Fig. 11. Top: gray-scale plot of the Major axis of the M_2 tidal current ellipse along the Dutch and German Wadden coast. Model results are obtained with a numerical model (ZUNO). Bottom: two cross sections along which the magnitude of the major axis of the M_2 tidal current ellipse is shown (for position of the barrier islands see Fig. 1). The two cross sections are shown in the top panel. White diamonds in the top panel show the seaward cross section while black diamonds show the landward cross section.

We have not compared the results of our combined wave–tide model with field data of Georgia Bight. One reason is that the wave climate is quite variable in this area and no results for $q_{(\mathrm{wave})}$ are available. Second, a detailed comparison between model results and observations is not possible at this stage, because the wave model and tide model assume different cross-sectional shape functions of bathymetric contours. This aspect deserves further study.

An important implication of our model hypothesis is that the spacing between successive inlets is determined by the wave and tidal current characteristics at sea (and not by the tidal range). The tidal currents and waves render the coastline unstable and determine the spots where the coastline might breach during storms. Note that our model is not designed to explain the existence of sequences of barrier islands. That would require the study of a model of a fully developed inlet system and using concepts that were already discussed in Bruun and Gerritsen (1960). In fact, whether the inlet system formed during a storm preserves on the long term depends on the competition between wave-driven littoral drift (that tends to close the channel) and tidal currents in the inlet that tend to widen its cross-sectional area.

7. Conclusions

In this paper, a simple model has been developed to study the evolution of alongshore periodic undulations of bathymetric contours. The new aspect of this study is the role of tides in the possible generation of such undulations. The model described in this study is a natural extension of the one-line models of Komar (1998), Ashton et al. (2001), Falqués (2003), Falqués and Calvete (2005) and Falqués (2006), which considered only the influence of waves on the initial evolution of the coastline. A linear stability analysis has been carried out, so no results are obtained that describe the

finite-amplitude behavior of undulations of the bathymetric contours.

The model shows that in the case that the wave induced sediment flux is zero the feedback between the location of the coastline and the alongshore sand flux is such that a straight coastline is unstable with respect to alongshore rhythmic perturbations with length scales longer than the shelf width. These perturbations migrate along the coast to the right (when viewing in the seaward direction). The physical mechanism resulting in growth or decay of coastline perturbations and their migration rates can be understood with vorticity dynamics. There is a competition between the cross-shore gradient of the mean cross-shore vorticity flux, which acts stabilizing, and alongshore gradient of the mean alongshore vorticity flux, which acts destabilizing. The width of the inner shelf determines the cross-shore length scale over which the cross-shore vorticity fluxes vary, while the wavelength of the perturbation determines the length scale over which the alongshore vorticity fluxes vary. If the length scale in the alongshore direction is smaller (larger) than the length scale in the cross-shore direction, the growth rate is positive (negative). The Coriolis force is responsible for the migration of the perturbations. This implies that on the southern hemisphere the perturbations will migrate to the left (when viewing in the seaward direction).

The tidal model has been combined with the wave model of Falqués and Calvete (2005), Falqués (2006) and has been applied to the Dutch coast. Effects of tides on the formation of undulations of the coastline turn out to be small for the southern Delta coast and for the central Dutch coast, but they are significant for the northern Wadden coast. Tidal currents and waves cause damping of undulations with large and small wavelengths, respectively, while both cause growth of undulations with intermediate wavelengths. Field data confirm the model prediction that for a constant wave climate the preferred length scale of undulations of the coastline is smaller in regions where the alongshore tidal currents are stronger. The present model thus suggests that it is the magnitude of the tidal current at sea that determines the length of barrier islands. This is an important difference with the conceptual model of FitzGerald (1996) which predicts that the length of barrier islands is inversely proportional to the tidal range. It should be kept in mind though that the present model only predicts locations along the barrier where breaching will probably occur during a storm.

Acknowledgements

This work has been conducted in the framework of the NWO-ALW Outer Delta Dynamics programme and was supported by NWO-ALW Grant No. 810.63.12 and 810.63.15. We thank Prof. A. Falqués for kindly providing the results of his wave model.

References

Ashton, A., Murray, A.B., Arnault, O., 2001. Formation of coastline features by large-scale instabilities induced by high-angle waves. Nature 414, 296–300.

Ashton, A., Murray, A.B., Ruessink, G., 2003. Initial tests of a possible explanation for alongshore sandwaves along the Dutch coast. In: Yanagi, T. (Ed.), Proceedings of the 3rd IAHR symposium. Terra Scientific Publishing Company, Tokyo, pp. 265–285.

Boyd, J.P., 2001. Chebyshev and Fourier Spectral Methods. Dover, New York, 688pp.

Bruun, P., 1954. Migrating sand waves and sand humps. In: Proceedings of the 5th Conference on Coastal Engineering. ASCE, New York, pp. 269–295.

Bruun, P., Gerritsen, F., 1960. Stability of coastal inlets. North-Holland Publishing Company, Amsterdam.

Calvete, D., Walgreen, M., de Swart, H.E., Falqués, A., 2001. A model for sand ridges on the shelf: effect of tidal and steady currents. Journal of Geophysical Research C 106, 9311–9338.

Ehlers, J., 1988. The Morphodynamics of the Wadden Sea. Balkema, Rotterdam, 397pp.

Falqués, A., 2003. On the diffusivity in coastline physics. Geophysical Research Letters 30 (21), 2119.

Falqués, A., 2006. Wave driven alongshore sediment transport and stability of the Dutch coastline. Coastal Engineering 53, 243–254.

Falqués, A., Calvete, D., 2005. Large scale dynamics of sandy coastlines: diffusivity and instability. Journal of Geophysical Research 110.

Falqués, A., Montoto, A., Iranzo, V., 1996. Bed-flow instability of the longshore current. Continental Shelf Research 16, 1927–1964.

FitzGerald, D.M., 1996. Geomorphic variability and morphologic and sedimentlogic controls on tidal inlets. Journal of Coastal Research 23, 47–71.

Grasmeijer, B.T., Kleinhans, M.G., 2004. Observed and predicted bed forms and their effect on suspended sand concentrations. Coastal Engineering 51, 351–371.

Komar, P.D., 1998. Beach processes and sedimentation. Prentice-Hall, Upper Saddle River, 544pp.

Luck, G., 1975. Der Einfluss der Schutzwerke der Ostfriesischen Inseln auf die morpologischen Vorgänge im Bereich der Seegaten und ihrer Einzugsgebiete. Tech. Rep. Heft 47, Technischen Univerisät Braunschweig.

Oost, A.P., de Boer, P.L., 1994. Sedimentology and development of barrier islands, ebb-tidal deltas, inlets and back-barrier areas of the Dutch Wadden Sea. Senckenbergiana Maritima 24, 65–115.

Pelnard-Considère, R., 1956. Essai de théorie de l'évolution des formes de rivages en plages de sable et de galets. In: 4th Journées de l'Hydraulique, Les Energies de la Mer. Soc. de Hydrotech. de France, Paris, pp. 289–298.

Roelvink, J.A., van der Kaaij, T., Ruessink, B.G., 2001. Calibration and verification of large-scale 2D/3D flow models phase 1. ONL coast and sea studies, project 2: Hydrodynamics and morphology. Tech. Rep. Z3029.10. 131pp., WL—Delft Hydraulics.

Ruessink, B., Jeuken, M.C.L., 2002. Dunefoot dynamics along the Dutch coast. Earth Surface Processes and Landforms 27, 1043–1056.

Sha, L.P., 1989. Variation in ebb-delta morphologies along the West and East Frisian Islands, The Netherlands and Germany. Marine Geology 89, 11–28.

Thevenot, M.M., Kraus, N.C., 1995. Longshore sand waves at Southampton Beach, New York: observation and numerical simulation of their movement. Marine Geology 126, 249–269.

Zimmerman, J.T.F., 1981. Dynamics, diffusion and geomorphological significance of tidal residual eddies. Nature 290, 549–555.

Zimmerman, J.T.F., 1992. On the Lorentz linearization of a nonlinearly damped tidal Helmholtz oscillator. In: Proceedings Koninklijke Nederlands Akademie van Wetenschappen, pp. 127–145.